Desalination and Water Treatment
www.deswater.com

doi:10.5004/dwt.2018.21993

106 (2018) 62–71
February

Mitigation of biofouling in polymer film heat transfer applications

Sebastian Pohl, Hans-Jörg Bart*

University Kaiserslautern, Chair of Separation Science and Technology Gottlieb-Daimler-Straße 44, D-67663 Kaiserslautern, Germany, Tel. +49 6312053775, email: sebastian.pohl@mv.uni-kl.de (S. Pohl), Tel. +49 6312052414, email: bart@mv.uni-kl.de (H.-J. Bart)

Received 6 October 2017; Accepted 5 February 2018

ABSTRACT

The thermal influence of progressing biofouling caused by *E.coli* K12 DSM 498 was investigated and correlated to intrinsic surface properties. The application of novel polymer film heat exchangers (polypropylene, polysulfone, polyethylene terephthalate, polyether ether ketone and polyamide) and their biofouling interaction was investigated and compared to stainless steel 304. Surfaces with low disperse surface free energy were found to mitigate the deposition of biofouling in laminar flow. The resistance of biofouling layers towards fluid shear forces was investigated and biofilms on surfaces with higher fractions of acid-base surface free energy were found to resist fluid shear forces more effectively. These observations were correlated to the high interaction of electron-donating and electron-accepting characteristics of substratum and microorganism in the wall-near region. Measurements of the thermal fouling resistance, as a degree of fouling layer thickness, in turbulent flow conditions showed that higher fractions of acid-base surface free energy of the substratum lead to an increased thickness of the biofouling layer. Based on these findings a cleaning-in-place method utilizing the flexibility of the disperse and non-polar polymer films to mechanically weaken fouling layers was successfully implemented for an *E.coli* K12 biofilm grown over 500 h in a falling film application.

Keywords: Biofouling; Heat exchanger; Fouling resistance; Surface properties; Fouling mitigation

1. Introduction

Biofouling as the unwanted settlement of bacteria, algae and macro organisms like mollusks, and the inherent forming biofilm of excreted extracellular polymeric substances (EPS) [1] is a large problem in medical, food packaging, marine and industrial applications [2]. Another common biofouling related problem is caused by the usage of untreated river water in industrial heat exchangers [3–5], which results in an additional heat transfer resistance decreasing the overall heat exchanger efficiency. The progressing layer formation increases the required pump capacity to overcome pressure loss due to increased friction and reduction of the inner diameter of tubing and flow channels in heat exchangers [6]. The resulting more moderate temperatures throughout all the different process sections, like tubing, heat exchangers and cooling towers, can lead to an enhancement of the biofouling process. Heat exchanger oversizing by 50–500%, heat loss and increased maintenance costs are the resulting fouling related costs [7].

In literature, several approaches can be found to prevent or reduce biofouling in heat exchangers, ranging from chemical to physical methods [8–10]. The choice of polymeric films in heat exchanger applications is connected to the promising instable bacterial adhesion properties [11] and the ability to withstand corrosion induced by inherent metabolic processes in the biofilm matrix. Development and application of heat exchangers utilizing thin polymers as heat transfer surfaces could therefore vastly increase the efficiency of heat transfer processes in environments characterized by high microbial loads. Some of the investigated polymers, in comparison to stainless steel (SS) 304, were already found to have promising low crystallization fouling tendencies [12]. In respect to their resistance to biofouling, a correlation between scaling, the biofouling process itself

*Corresponding author.

and the surface properties of polymers could be shown [13]. An experimental investigation of biofilm formation and the resulting thermal fouling resistance is given for different polymer surfaces varying in surface chemistry and compared to SS 304 in order to increase the understanding of biofouling interaction mechanisms in thermal applications. The resistance of the developed *E.coli* K12 DSM 498 biofilms against shear forces was measured and correlated to the chemical composition of the substrata. Data on this surface specific interaction mechanism could lead to the development of design heat transfer surface utilizing multiple mitigation techniques. The mitigation of microorganisms, measured as the exceeding of the inherent adhesion forces, due to chemical-free cleaning-in-place (CIP) mechanisms for flexible heat transfer surfaces is discussed and investigated experimentally.

2. Materials & methods

2.1. Investigated surfaces

In this work, seven different polymer films were tested against stainless steel 304 (Metall Ehrnsberger, Teublitz-Münchshofen, Germany) as commonly used basis material for industrial heat exchanger construction. Three different polyether ether ketones (PEEK), one polymer being semi-crystalline (LITE TK) and the other two additionally containing 30% mineral filler (LITE TKT30, APTIV® 1103), polyamide 12 (PA12) (LITE PA12) from Lipp-Terler GmbH, polysulfone (PSU) and polypropylene (PP) from (Pütz GmbH + Co. Folien KG, Taunusstein, Germany) as well as polyethylene terephthalate (PET) (Dr D. Müller GmbH, Ahlhorn, Germany) were used as substrates. The composition of the mineral filler in LITE TKT 30 and APTIV® 1103 (Victrex Euro GmbH, Hofheim Taunus, Germany) were labeled as talc by the manufacturers. In case of e.g. PEEK the wall thickness of the polymer film must be about 25 µm ($\lambda \approx 0.25$ W m^{-1} K^{-1}) in order to achieve similar heat transfer coefficients as stainless steel with approximately 1–1.5 mm ($\lambda \approx 10$–15 W m^{-1} K^{-1}). Application of special filler materials like graphite or minerals could significantly enhance the thermal conductivity of the polymer films whilst retaining the beneficial fouling related chemical surface properties [14].

Prior to testing, all substrata were cleansed with deionized (DI) water, dried for two hours at 50°C and further dried in a desiccator for one hour. The films were then subsequently weighed with an earthed micro balance. After conducting the experiments, the different surfaces were dried again similar to sample preparation. The accumulated dry biomass resulted from the difference in weight before and after the experiments.

2.2. Media

E. coli K12 DSM 498 was in previous investigations found to be a valid model bacterium for the interaction of microorganisms and substrata [15] and showed qualitative similar deposition behavior than complex biofilms from the German river Rhine. It was cultivated with LB Miller nutrient solution containing 10 g L^{-1} tryptone, 10 g L^{-1} NaCl and 5 g L^{-1} yeast extract. The preparatory bacterial type culture was grown in the undiluted nutrient solution. This preparatory culture was further incubated overnight in a heated shaking bath at 37°C and 120 rpm in order to increase bacterial growth. The optical density (OD) was constantly monitored with a photometer (Lambda Bio+, PerkinElmer, Waltham, MA, USA) at an excitation wavelength of 600 nm, which is the recommended wavelength when analyzing the OD of *E. coli* suspensions [16].

3. Experimental procedure

3.1. Determination of the surface properties

The surface properties of the substrata, namely the surface free energy including the composition of polar acid-base components [17] were obtained *via* measuring the static contact angles of 4 different test liquids according to the standard sessile drop method [18]. The test liquids were DI water, diiodomethane, formamide and ethylene glycol. The composition of the surface tension of the test liquids is displayed in Table 1, in which γ_{lv}^{LW} denotes the apolar Lifshitz-van der Waals component, γ_{lv}^{AB} denotes the polar acid-base component, γ_{lv}^{+} denotes the electron-accepting component and γ_{lv}^{-} denotes the electron-donating component of the liquid surface free tension, that can be measured *via* the pendant drop technique [19].

The contact angles θ of the test liquids correlate with the surface free energies of the substrate according to the Young's equation [Eq. (1)] and depend on the thermodynamic equilibrium of the participating phases of solid *s*, liquid *l* and surrounding vapor phase *v*.

$$\gamma_{lv}\cos\theta = \gamma_{sv} - \gamma_{sl} \tag{1}$$

According to the acid-base theory, the surface free energy of the solid-liquid interface can be written as follows [7]:

$$\gamma_{sl} = \left(\sqrt{\gamma_{sv}^{LW}} - \sqrt{\gamma_{lv}^{LW}}\right)^2 + 2\left(\sqrt{\gamma_{sv}^{+}\gamma_{sv}^{-}} + \sqrt{\gamma_{lv}^{+}\gamma_{lv}^{-}} - \sqrt{\gamma_{sv}^{+}\gamma_{lv}^{-}} - \sqrt{\gamma_{sv}^{-}\gamma_{lv}^{+}}\right) \tag{2}$$

For the calculation of the surface free energy according to van Oss et al. [17], contact angle measurements of at least three different liquids, of which two must be polar with known surface tension composition, have to be conducted

Table 1
Surface tension components (in mN m^{-1}) of the test liquids according to the acid-base model [18]

	γlv	γlv^{LW}	γlv^{AB}	γlv^{+}	γlv^{-}
Water (DI)	72.8	21.8	51.0	25.5	25.5
Diiodomethane	50.8	50.8	0	0	0
Formamide	58.0	39.0	19.0	2.28	39.6
Ethylene glycol	48.0	29.0	19.0	1.92	47.0

in order to solve Eq. (3) being derived from the combination of Eqs. (1) and (2).

$$(1+\cos\theta)\cdot\gamma_{lv}=2\left(\sqrt{\gamma_{sv}^{LW}\gamma_{lv}^{LW}}+\sqrt{\gamma_{sv}^{+}\gamma_{lv}^{-}}+\sqrt{\gamma_{sv}^{-}\gamma_{lv}^{+}}\right) \quad (3)$$

The acid-base fraction can then be determined by the combination of electron-donating and electron accepting fractions of the surface free energy according to Eq. (4) [17]:

$$\gamma_i^{AB}=2\cdot\sqrt{\gamma_i^{+}\cdot\gamma_i^{-}} \quad (4)$$

3.2. Biofilm channel

The generation of biofilms for the investigation of interaction and adhesion experiments was conducted in a modified biofilm screening apparatus known from literature (Fig. 1) [15,20]. The channels were composed of poly methyl methacrylate, were machine-cut and have an inner length of 12 cm and width of 3 cm. The upper and lower half of the flow channels were sealed with gaskets of polytetrafluoroethylene. The entrance and outlet length of 2 cm was shaped in the form of a trapezium in order to expand the inlet width of 1 cm to 3 cm. The channel height of 1 cm was chosen in order to diminish the hydrodynamic boundary effects. The flow channels were fixed in a mount allowing to adjust the channels in angles between 90° and 0° in order to validate the influence of sedimentation and operated with a multi-channel peristaltic pump. The detailed geometry and its validity to use for laminar investigations was derived in preceding CFD flow simulations with the commercial software ANSYS Fluent® (16.0, ANSYS Germany GmbH, Darmstadt, Germany). The flow channels were operated vertically and in parallel from the same batch feed at identical process parameters flow velocity and temperature in order to have direct comparability between the respective substrata [15].

After the OD of the preparatory culture reached 0.6, which resembles ~10^8 cells per mL in the standardized cuvette, 50 mL of the bacterial culture were transferred into the respective 1:10 diluted LB-Miller batch media. This batch was subsequently used as feed for the flow channels and was operated in a recirculating mode. The NaCl concentration was kept undiluted for the cultivation in order to avoid osmotic stress. The flow rate was set to 100 mL min^{-1} for each channel, which results in a laminar flow regime with Reynolds number of about *Re* = 110–120. More detailed microbiological investigations e.g. staining cells and gravimetric analyzes over time were performed in separate experiments with similar channel setup [13,15,21], but were not specifically addressed in this work due to the macroscopic approach of the presented measurement techniques.

3.3. Shear stress measurement

Measuring adhesion forces between single microorganisms or complete biofilms is challenging, as the viscous behavior of the whole biofilms is different than for the single microorganism due to its embedding into the matrix of extracellular polymeric substances (EPS). Therefore numerous continuous liquid flow methods are described in literature to generate shear forces induced by a moving liquid acting on the fouling layers and leading to partial or complete removal of the biofilm. A comparison was given by Bos et al. [22] with methods reaching from flow channels, stagnation point flow, slides and rotating disks that are still used today and have all their respective advantages and disadvantages.

The rotating disk in a stagnating liquid, which was investigated by Fowler and McKay [23], was chosen as screening method, as the usage of biofilms from the biofilm flow reactors/channels was most accessible. Two samples were fixed onto both sides of the disk surface with double sided adhesive tape [13] (Fig. 2).

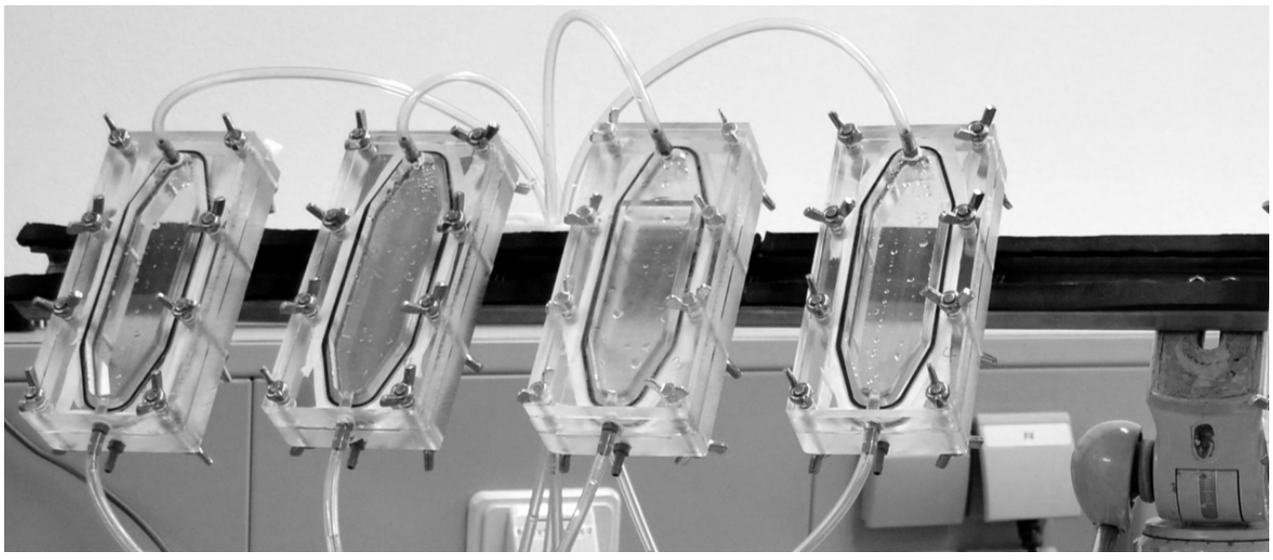

Fig. 1. Adjustable test rig of the flow channels.

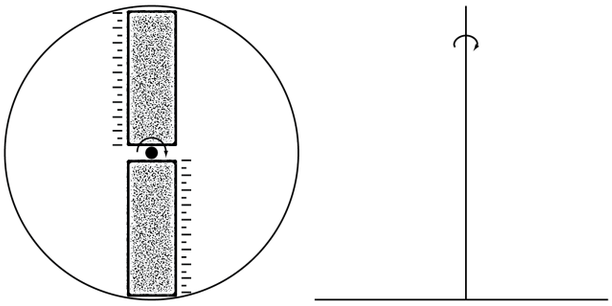

Fig. 2. Schematic of the horizontal rotating disk setup including sample positioning.

Due to the rotation of the disk a defined fluid induced shear stress is present at each point in relation to the distance from the rotation axis. If the shear stress exceeds the adhesion forces of the biofilm at any given point a clear detachment line should be visible. By increasing the rotational speed, the detachment line would then move towards the central axis but should result in identical detachment shear stress at each threshold line. Under these conditions, the wall shear stress τ varies linearly [Eq. (5)] with the radial position according to García et al. [24] for laminar flow conditions of $Re < 3 \cdot 10^5$ [25] defined in Eq. (6). In Eqs. (5) and (6), ω is defined as the rotational speed of the disk and r_a as the radius of the disk.

$$\tau = 0.8r\sqrt{\rho\eta\omega^3} \tag{5}$$

$$Re = \frac{r_d^2 \omega \rho}{\eta} \tag{6}$$

The experiments were conducted with *E. coli* K12 biofilms grown over two weeks with laminar flow conditions (*Re* = 110–120) as previously described. The nutrient solution was changed every three days. At least two experiments per substratum were conducted and investigated with at least six different rotational speeds between about 15 and 52 rad s^{-1} for 1 min. The radius of the disk was 0.125 m and ambient temperatures were 25°C.

3.4. Fouling resistance measurement

The overall heat transfer coefficient *U* in any heat transfer process can be written as the combination of the separate heat transfer coefficients α_i, acting as separate thermal resistances, from the cold side to the hot side in heat transfer applications [Eq. (7)]. The formation of any fouling layer *f* will pose as additional thermal resistance and thus lowering the thermal efficiency of any heat transfer process.

$$\frac{1}{U} = \frac{1}{\alpha_1} + \frac{s_w}{\lambda_w} + \frac{1}{\alpha_2}\left(+\frac{s_f}{\lambda_f}\right) \tag{7}$$

In Eq. (7) α_1 denotes the heat transfer coefficient from the liquid to the heat transfer wall, s_w the thickness of the wall, λ_w the thermal conductivity of the wall and the possible influence of any given fouling layer. The thermal conductivity of most biofilms can be taken as $\lambda_f = 0.5–0.7$ W m^{-1} K^{-1}, but strongly depends on the water/organic ratio in the biofilm [4].

The resulting fouling resistance R_f due to fouling layer formation is defined as the reciprocal difference between the overall heat transfer coefficient of the clean surface U_0 and of the surface including fouling layer U_f. The fouling layer thickness s_f therefore correlates with the density ρ_f and the biomass m_f per fouled area A_f [Eq. (8)].

$$R_f = \frac{1}{U_f} - \frac{1}{U_0} = \frac{s_f}{\lambda_f} = \frac{m_f}{\rho_f \cdot A_f \cdot \lambda_f} \tag{8}$$

The investigation of thermal influence of biofouling on the several substrata was performed in a fouling screening setup. The schematic of this temperature controlled stirred vessel utilizing a pitched blade agitator can be seen in Fig. 3. In this setup, flat substrata of various materials can be fixed onto a copper heating block by using an insulating frame. The copper block was placed in a 10 mm thick polyoxymethylene (POM) encasing to insulate the remaining three sides. Inside the copper block were bore holes for two Pt 100 resistance thermometers right below the interface between copper and rear side of the investigated surface. Two additional bore holes in the middle of the copper block were equipped with power controlled heating cartridges (type HLP, Türk + Hillinger GmbH, Germany) and fixed with thermal conductivity paste. Thus the surface temperature of the surface area of A = 0.0024 m^2 could be controlled precisely by approximating the influence of fluid flow velocity above the substratum via the so called Wilson plot [26] but remained constant for the given investigation in this work. The vessel was filled with 1.6 L of undiluted LB-Miller nutrient solution and 50 mL of the preparatory bacterial solution was added at the experiment start after the nutrient solution reached thermal equilibrium.

The resulting temperatures inside the vessel and inside the cooling jacket as well as the turbidity and pH value were monitored constantly. The resulting measured bulk and surface temperatures are, in addition to the surface characteristics, key parameters for the biofilm development. The fluid characteristics inside the stirred vessel were adjusted *via* the rotational speed of the rotor and were described by the Reynolds number *Re*. In Eq. (9) *n* denotes the number of rotations, d_r the diameter of the rotor, ρ_l the density of the liquid and η_l the dynamic viscosity of the liquid. Laminar flow conditions prevail for $Re < 10^5$ [27].

$$\mathrm{Re} = \frac{\rho_l \cdot n \cdot d_r^2}{\eta_l} \tag{9}$$

Most biofouling processes also experience certain induction period at the beginning, as single microorganism colonies adhere to the surfaces but are not able to form a continuous layer that would represent a fouling resistance. Therefore the fouling fragments act as additional roughness or turbulence generator, which reduces the viscous laminar sub-layer and in return promotes the heat transfer from the wall to the fluid without being able to form a continuous layer. In technical applications the fouling resistance, as direct parameter of the fouling layer condition, is often replaced by the cleanliness factor *CF* that is the direct ratio

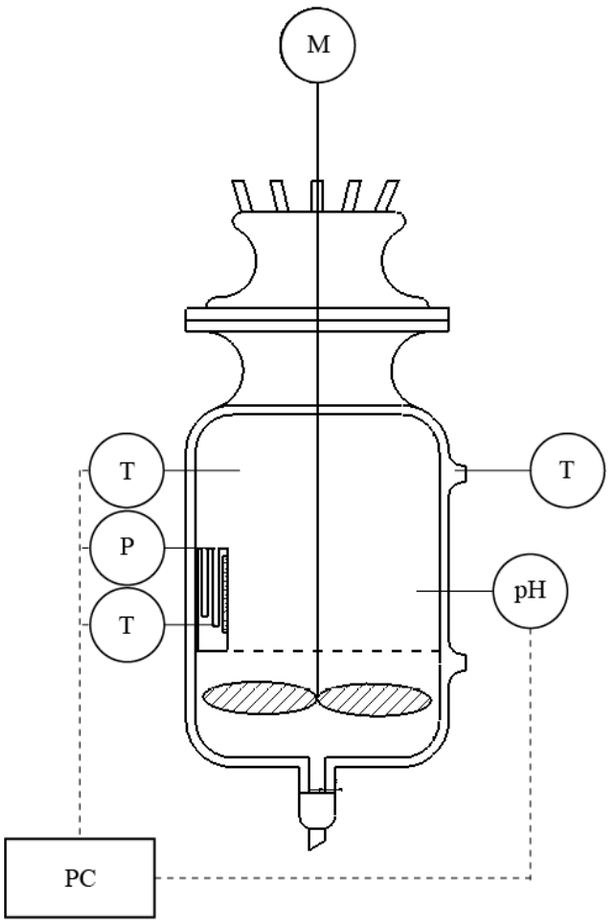

Fig. 3. Schematic of the temperature controlled stirre vessel including heat transfer surface.

between U_f and U_0 and gives information about the persisting thermal efficiency of the heat transfer surface [Eq. (10)].

$$CF = \frac{U_f}{U_0} \tag{10}$$

3.5. Falling film apparatus and CIP measurement

The thermal influence of biofouling was also investigated on a larger heat transfer area of PEEK with $A = 0.052\ m^2$. The schematic of this setup can be seen in Fig. 4. The thin polymer film was supported by a point welded stainless steel spacer grid in order to prevent excessive bulging due to the flow from the heating side. The counter-current flow operation without phase change was operated with water as heat transfer fluid. The falling liquid film side contained 25 L of 1:10 diluted LB-Miller nutrient solution incubated with *E. coli* that was refilled daily in order to provide sufficient nutrients and to balance liquid losses due to evaporation. Gear type pumps as well as the transient measurement of inlet and outlet temperatures *via* NiCr-Ni thermocouples (type K) and the insulation of the setup ensured the evaluation of reproducible mass and energy balances and equal liquid distribution. The falling film Reynolds number was $Re_{ff} = 379$, which is below the critical Reynolds number $Re_{f,crit} = 400$ for the transition between laminar and turbulent flow and was set to 2.8 L min^{-1}. The inlet temperatures of the liquid falling film were 37°C and for the heating side 52°C.

4. Results

4.1. Surface properties

Table 2 shows the measured surface free energies of the substrata that were determined via sessile drop contact

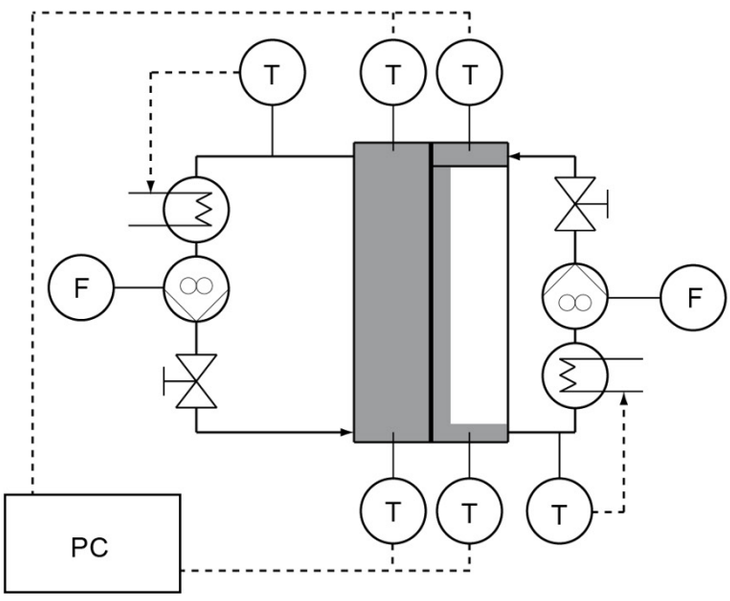

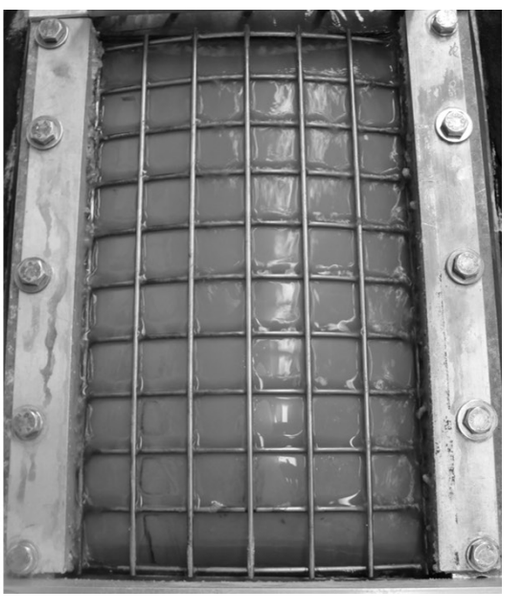

Fig. 4. Schematic and front view of the falling film plate heat exchanger.

Table 2
Surface free energies (in mN m^{-1}) of the investigated substrata according to the acid-base theory

	γ_{sv}^{LW}	γ_{sv}^{+}	γ_{sv}^{-}
PP	25.98	0.06	1.05
PA 12	27.74	1.65	11.74
PSU	27.88	0	14.35
PEEK (1103)	33.26	2.2	4.98
SS 304	37.15	0	5.80
PEEK (TKT30)	38.75	0	4.22
PEEK	39.59	0	3.65
PET	41.91	0	6.35

angle measurements of the four test liquids. Surface energy fractions below 10^{-2} were depicted as zero but were nevertheless used for interaction calculations. The resulting acid-base fractions can be calculated from Eq. (4).

It can be seen that for all substrata the disperse Lifshitz-van der Waals fraction dominates the total surface free energy, whilst the electron-accepting is close to zero for many substrata, which correlates well with literature [17,28]. The roughness was also investigated via tactile scanning and white light interferometry measurements but its influence showed to be negligible for the respective substrata with mean arithmetic roughness between 0.04 and 0.87 µm [21] compared to the measured mean equivalent spherical diameter $d_{E.coli\ K12}$ = 0.8 µm.

4.2. Resistance against shear stress

Fig. 5 shows the resistance against wall shear stress for the respective substrata, which was necessary to detach the two week old *E. coli* K12 biofilm grown under laminar flow conditions, in relation to the acid-base fraction of the respective surface free energies.

4.3. Fouling resistance

The results of the indirectly measured fouling resistance for PEEK, PEEK (TKT30), PA12 and SS 304 can be seen in Fig. 6. It can be seen that the substrata show sigmoidal progression of the fouling resistance and respective asymptotic fouling resistance after 64 h. This experimental duration was chosen as the microorganisms were still vital and not in a degenerative state in the undiluted nutrient solution.

Fig. 6 also shows that the induction period with $R_f < 0$ varies in value and duration for the substrata. The temporary increase of heat transfer efficiency can be explained as the biofilm exists in smaller colonies on the surface that are not yet able to form a continuous film that would pose a thermal resistance [21]. The small microorganisms on the other hand increase the wall near turbulence of the fluid flow and therefore promote the heat transport α from the wall to the fluid, resulting in a temporarily negative fouling resistance R_f. In the case of polymers where the biofilm shows higher thermal conductivities of approximately

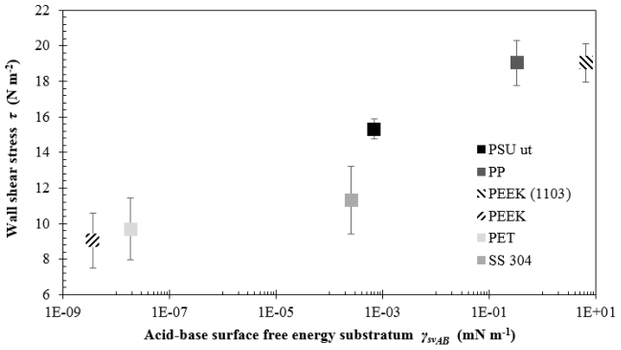

Fig. 5. Measured resistance against shear stress of a two week old *E. coli* K12 biofilm grown under laminar flow conditions in relation to the acid-base fraction of the surface free energy of the investigated substrata.

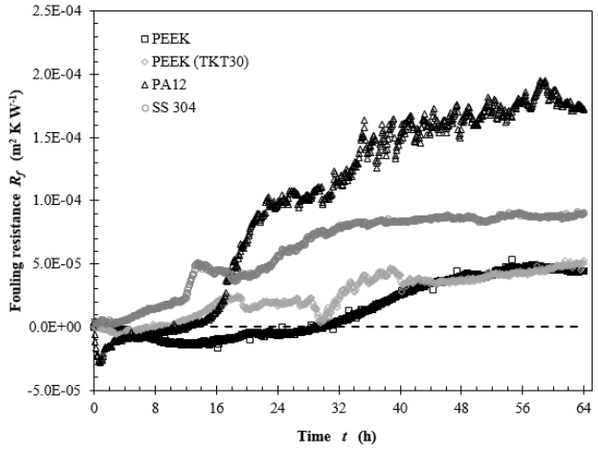

Fig. 6. Fouling resistance over time in undiluted LB-Miller nutrient solution at T_{wall} = 40°C and T_{bulk} = 25°C and Re = 59100.

water with λ = 0.5–0.7 W m^{-1} K^{-1} heat transfer might also be increased due to locally higher heat transfer coefficients. The induction period also varies between measurements of a single surface although shape and asymptotic fouling resistance show comparative values. Taking the thermal conductivity of the biofouling layer on all substrata as constant, the fouling resistance would directly correlate with the fouling layer thickness. Therefore, the biofouling layer would be thickest on PA12 and thinnest on both PEEK and PEEK (TKT30).

4.4. Cleaning-in-place (CIP)

In order to retain the thermal effectivity in heat transfer applications, periodically cleaning procedures (chemical or mechanical) are necessary to remove the fouling resistances. The possibility of implementing a CIP method for the flexible polymer films in the falling film apparatus was tested for *E.coli* K12 after 500 h of continuous growth in 1:10 diluted LB-Miller nutrient solution. The falling film containing the microorganisms was switched off for 5 min while retaining

the wall temperature by the heating agent in order to predry the biofilm. Then the pressure of the heating fluid in the falling film apparatus was decreased by switching off the pump resulting in a relaxation of the flexible polymer film and immediately switching it on again. The liquid falling film was switched on simultaneously and after the polymer film was completely wetted, the cleaning procedure was repeated 2 more times. The fouling resistance over time, as well as the influence of the CIP procedure, is depicted in Fig. 7.

5. Discussion

5.1. Laminar interaction of E. coli with substrata

It was found that the mean dry biomass directly correlated with the disperse Lifshitz-van der Waals fraction of the surface free energy for all polymers but not for SS 304 (Fig. 8). An increase in disperse surface free energies correlated also with an increased deposition of biomass possibly due to the long-range disperse interaction with the microorganisms (Fig. 5) which corresponds to findings in literature [29,30]. SS 304 most likely showed disproportionately high deposition as the zeta potential at pH = 7 was measured to be close to the iso electric point, meaning that no electrostatic repulsion between the also negatively charged microorganisms occurred and solely disperse attraction was present. The polymers all showed highly negative zeta-potentials at these pH values analogous to the experiment.

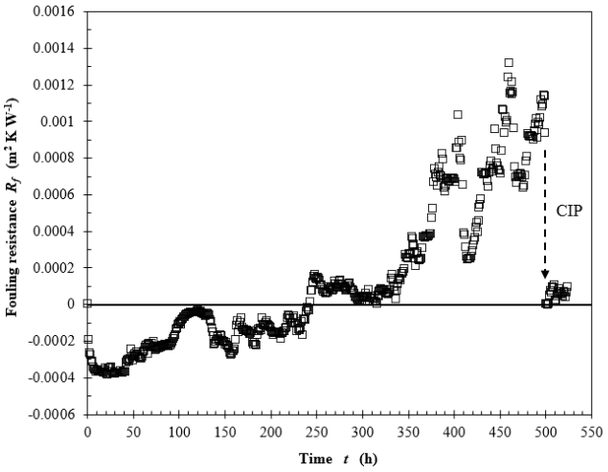

Fig. 7. Influence of three CIP cycles on the fouling resistance of *E. coli* K12 in 1:10 LB-Miller nutrient solution in a falling film.

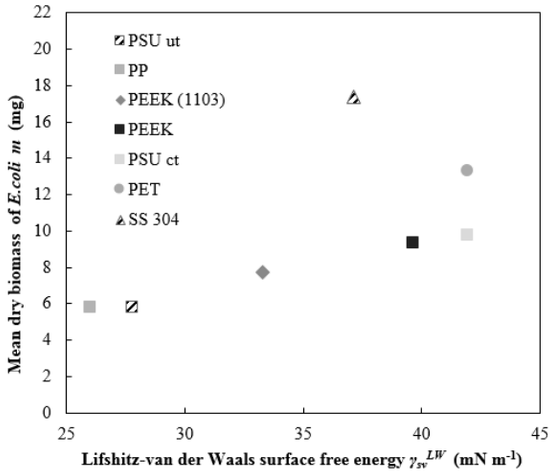

Fig. 8. Mean dry biomass in relation to the disperse Lifshitz-van der Waals surface free energy.

5.2. Resistance against shear stress

Fig. 5 shows that the resistance against shear stress seems to correlate with the acid-base fraction of the substrata surface free energy. Similar correlation with the disperse Lifshitz-van der Waals surface free energy as found concerning the deposited dry biomass [13] was not found. This would mean, that a polar surface forms stronger adhesion forces between microorganism and substratum. Supporting evidence for these findings are the short-ranged polar forces influence adhesion in the wall-near region and correlate with the acid-base free energy of adhesion based on thermodynamic interactions [Eq. (11)], which was also investigated by other work groups [2,31]. Eq. (11) resembles the interaction and cross-interaction of the three phases (microorganism *mv*, immersion liquid *lv* and substratum *sv*) concerning their electron-donating and electro-accepting fractions of the surface free energy.

A non-polar surface [according to Eq. (4)] is in most cases based on significant electron-donating surface free energy but no electron-accepting surface free energy. Given a polar liquid like water and a microorganism with similar significant electron-donating surface free energy [13], this microorganism would experience repulsion due to the interaction of electron-donating surface free energies. Even a slight increase in electron-accepting surface free energy of either substratum or microorganism would therefore significantly reduce repulsion in the wall-near region and so adhesive properties would dominate the interaction process [Eq. (11)]. This interaction would result in an increased resistance against shear stress as can be seen from Fig. 6.

5.3. Fouling resistance

When comparing the asymptotic fouling resistance (Fig. 6) with the acid-base fraction of the respective substrata, it was found that an increasing acid-base content lead to an excessive fouling layer thickness (Fig. 9). This would mean that especially in turbulent flow conditions or adhesion processes where fluid forces are relevant in general, the resistance against shear stress is the governing factor of the resulting fouling layer thickness. These results would therefore be in correlation with the previously described findings concerning the resistance against shear forces. The asymptotic fouling layer in these experiments would be defined by the acid-base fraction according to $R_f^{\infty} = 10^{-4} (\gamma_{sv}^{AB})^{0.0624}$ as regression with least squares fitting. How this polarity of the substrata affects the biofilm formation of thicker fouling layers remains currently unclear. The substrata properties should, from a conceptual point of view, mostly affect the

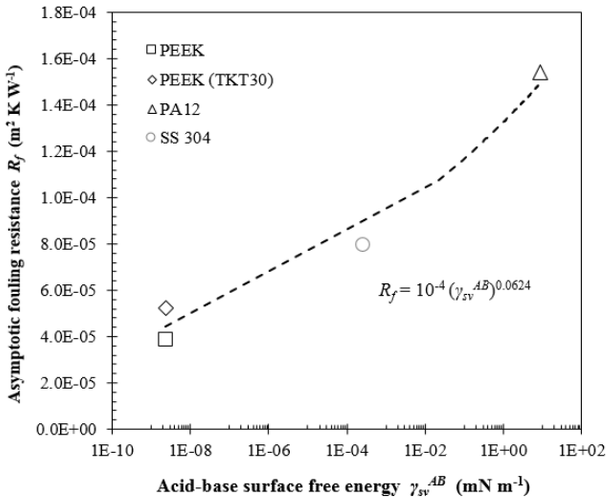

Fig. 9. Asymptotic fouling resistance in relation to the acid-base surface free energy of the substrata.

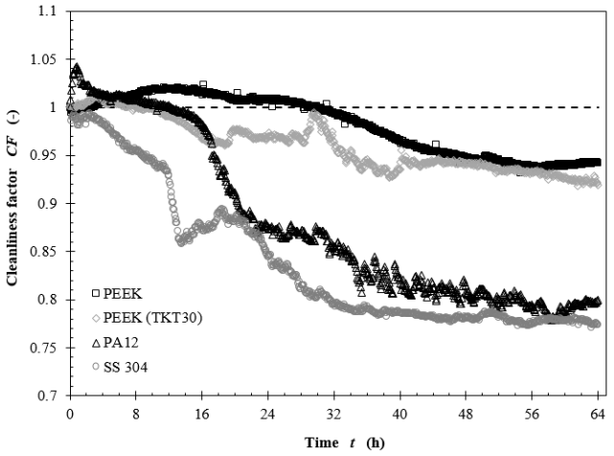

Fig. 10. Cleanliness factor ***CF*** in relation to the experimental duration.

primary adhesion mechanism. Progressing fouling formation would therefore depend on the properties of the then formed thin conditioning fouling layers. Experiments with the *E. coli* K12 strain showed that the measurable properties of the fouling layers for several substrata (roughness and surface free energy) homogenized over the course of up to 44 d of experiment [21]. Nevertheless, significant property differences were investigated for the respective substrata in intervals of up to four days. This could mean that the polarity of the substrata would not only influence the primary adhesion mechanism but also the physiology of the biofilm and its chemical composition. This altered biofilm physiology could in return be the reason why varying fouling resistances, respectively biofilm heights, correlated with the substrata polarity.

The fouling resistance R_f itself does not allow for the simple comparison of various materials with differing thermal conductivities concerning the influence of fouling layers, as a direct comparison is solely valid for identical materials. The fouling resistance itself is solely an indirect parameter for estimating the fouling layer thickness. The low thermal conductivity of the biofouling layer has to be seen as thermal bottleneck especially for materials with higher thermal conductivities e.g. SS 304. The cleanliness factor *CF* as direct ratio of the respective clean and fouled heat transfer coefficient allows in addition to the technical comparability to investigate the necessary oversizing of the heat exchanger. The *CF* over time for the selective substrata is depicted in Fig. 10.

Excessive biofouling is on the benchmark SS 304 surface with a *CF* of about 0.77 after 64 h of experiment, although PA 12 was in the same range with 0.80. The resulting hypothetical excess heat transfer surface in a heat exchanger in order to maintain the respective heat transfer efficiency would be 30% for SS 304 and 25% for PA 12. The required overdesign for PEEK with *CF* = 0.94 and PEEK (TKT30) with *CF*= 0.92 would not exceed 8% for the same initial surface temperatures of 40°C and turbulent flow with *Re* = 59100. The SS 304 surface did not show any induction period, whilst all of the polymers had induction periods of varying length. Especially PEEK retained its thermal efficiency over approximately 30 h. These results correlate qualitatively well with investigations concerning $CaSO_4$ crystallization fouling in previous work [32] and show the strong relation between substrata properties and various forms of fouling. The calculations also show that although R_f of SS 304 was between the selective polymer surfaces, the loss in thermal efficiency was largest, requiring for excessive heat transfer surface over design in order to attribute for the biofouling layer formation of low thermal conductivity.

5.5. Cleaning-in-place (CIP)

The CIP procedure prove to be very effective after three cleaning cycles. Based on visual inspection during the cleaning procedure most macroscopic detachment occurred during the first cleaning cycle. Due to the lower concentration of microorganisms the induction time significantly increased compared to the experiments with undiluted nutrient solution. The mechanical stress on the predried biofilm was sufficient to detach it from both polymer film and most of the spacer grid. The fouling resistance reached its initial state but no induction period followed. Whilst most of the fouling layers could be removed, and therefore significantly decreasing the thermal resistance of the biofilm, a thin film seemed to persist on the surface preventing the formation of single microorganism colonies that would result in another induction period. Possible adaptation of the remaining thin biofilm to shear stress for continuous cleaning procedures was not investigated. The remaining fouling fragments can have significant influence on the surface free energy and zeta potential [33] and could also alter the following interaction mechanism. The current fouling experiments ended after approximately 24 h with the cleaned surface and therefore no direct information can be currently given on the experimentally measured interaction with the altered substrata over time. It should also be stated that whilst starting with only the *E. coli* K12 species, due to the semi-open setup contamination of the nutrient solution

further microorganisms developed in contrast to the batch experiments, as was seen in microscopic investigations. This prohibits the direct comparison of these results or the developed fouling resistances. As solely the possibility to clean biofouling layers was shown and discussed, this cross-contamination was not validated in the current experiments but could be investigated in future work.

6. Conclusions

The investigation of *E. coli* K12 DSM 498 biofouling as thermal resistance, its correlation to the properties of the interacting substrata as well as measurements to exceed the respective adhesion forces lead to the following conclusions:

(1) The disperse Lifshitz-van der Waals fraction of the surface free energy of the substrata correlated well with the deposited dry biomass for surfaces with similar electrostatic properties. SS 304 with its zeta potential close to its isoelectric point at pH = 7 resulted in a disproportional high biomass deposition than would have been expected solely on the basis of the disperse surface free energy.
(2) The measured resistance against fluid shear forces for laminar grown biofilms, compared to the acid-base fraction of the surface free energy of the substrata, showed that an increased polarity resulted in higher adhesion forces. Biofilms on PEEK (1103) were most resistant against shear forces whilst detachment on PEEK occurred for low shear forces.
(3) The thermal, asymptotic fouling resistances at turbulent flow conditions and undiluted LB-Miller nutrient solution correlated with the polar acid-base fraction of the surface free energy of the substrata. In more turbulent systems the resistance against shear forces appeared to be dominant against the long-distance interaction of disperse mechanisms and resulted in thicker biofouling layers. The biofilm thickness on PEEK was lowest whilst PA12 showed excessive fouling formation.
(4) A CIP method was successfully tested with a flexible PEEK film by varying the bulging of the polymer film by changing the pressure of the heating side. This mechanical stress coupled with short drying and washing intervals was able to restore heat transfer coefficient values of the initial clean surface.

List of symbols

A — Surface area (m²)
CF — Cleanliness factor (–)
d_r — Rotor diameter (m)
m — Mass (g)
n — Number of rotations (–)
OD — Optical density (–)
r — Radius (m)
R_e — Reynolds number (–)
R_f — Fouling resistance (m² K W^{-1})
s — Layer thickness (m)
T — Temperature (K, °C)
t — Time (h)
U_i — Overall heat transfer coefficient (W m^{-2} K^{-1})

Greek

α_i — Heat transfer coefficient (W m^{-2} K^{-1})
γ_{sv} — Surface free energy substratum (mN m^{-1})
γ_i^+ — Electron-acceptor of the surface free energy (mN m^{-1})
γ_i — Electron-donor of the surface free energy (mN m^{-1})
γ_i^{AB} — Acid-base surface free energy (mN m^{-1})
γ_i^{LW} — Lifshitz-van der Waals surface free energy (mN m^{-1})
γ_{mv} — Surface free energy microorganism (mN m^{-1})
γ_{sl} — Interfacial energy (mN m^{-1})
γ_{lv} — Surface tension liquid (mN m^{-1})
η — Dynamic viscosity (kg m–1 s^{-1})
θ — Contact angle (°)
λ — Thermal conductivity (W m^{-1} K^{-1})
ρ — Density (kg m^{-3})
τ — Wall shear stress (N m^{-2})
ω — Rotational speed (rad s^{-1})

References

[1] A. Roosjen, H.C. van der Mei, H.J. Busscher, W. Norde, Microbial adhesion to poly (ethylene oxide) brushes: influence of polymer chain length and temperature, Langmuir, 20 (2004) 10949–10955.
[2] I. Banerjee, R.C. Pangule, R.S. Kane, Antifouling coatings: recent developments in the design of surfaces that prevent fouling by proteins, bacteria and marine organisms, Adv. Mater., 23 (2011) 690–718.
[3] W.G. Characklis, Biofouling - effects and control, in: Proc. International Workshop on Industrial Biofouling and Biocorrosion. Biofouling and Biocorrosion in Industrial Water Systems, 1991, pp. 7–27.
[4] S.E. Coetser, T.E. Cloete, Biofouling and biocorrosion in industrial water systems, Crit. Rev. Microbiol., 31(4) (2005) 213–232.
[5] S. García, A. Trueba, L.M. Vega, E. Madariaga, Impact of the surface roughness of AISI 316L stainless steel on biofilm adhesion in a seawater-cooled tubular heat exchanger-condenser, Biofouling, 32(10) (2016) 1185–1193.
[6] R. Steinhagen, H. Müller-Steinhagen, K. Maani, Problems and costs due to heat exchanger fouling in new zealand industries, Heat Transfer Eng., 14 (1993) 19–30.
[7] H. Müller-Steinhagen, Verminderung der Ablagerungsbildung in Wärmeübertragern, in: VDI-Wärmeatlas 11. ed., Berlin, Heidelberg: Springer, 2013, pp. 91–121.
[8] T.R. Bott, Techniques for reducing the amount of biocide necessary to counteract the effects of biofilm growth in cooling water systems, Appl. Therm. Eng., 18(11) (1998) 1059–1066.
[9] T.R. Bott, Potential physical methods for the control of biofouling in water systems, Chem. Eng. Res. Des., 79 (2001) 484–490.
[10] A. Trueba, S. García, F.M. Otero, L.M. Vega, W. Madariaga, The effect of electromagnetic fields on biofouling in a heat exchange system using seawater, Biofouling, 31(1) (2015) 19–26.
[11] L. Li, Z.Wang, L.C. Rietveld, N. Gao, J. Hu, D. Yin, S. Yu, Comparison of the effects of extracellular and intracellular organic matter extracted from *Microcystis aeruginosa* on ultrafiltration membrane fouling: dynamics and mechanisms, Environ. Sci. Technol., 48(24) (2014) 14549–14557.

[12] C. Dreiser, L.J. Krätz, H.J. Bart, Kinetics and quantity of crystallization fouling on polymer surfaces: impact of surface characteristics and process conditions, Heat Transfer Eng., 36 (2015) 715–720.
[13] S. Pohl, M. Madzgalla, W. Manz, H.J. Bart, Interaction of *E.coli* and autochthonous river water microorganisms with polymers in heat transfer applications, in: H. Müller-Steinhagen, H.U. Zettler, Proce. International Conference on Heat Exchanger Fouling and Cleaning XII, Aranjuez/Madrid, Spain, 2017, accepted.
[14] Y.P. Mamunya, V.V. Davydenko, P. Pissis, E.V. Lebedev, Electrical and thermal conductivity of polymers filled with metal powders, Eur. Polym. J., 38 (2002) 1887–1897.
[15] S. Pohl, M. Madzgalla, W. Manz, H.J. Bart, Biofouling on polymeric heat exchanger surfaces with *E. coli* and native biofilms, Biofouling, 31 (2015) 699–707.
[16] G. Sezonov, D. Joseleau-Petit, R. D'Ari, Escherichia coli physiology in Luria-Bertani broth, J. Bacteriol., 189(23) (2007) 8746–8749.
[17] C.J. van Oss, R.J. Good, M.K. Chaudhury, The role of van der Waals Forces and hydrogen bonds in "hydrophobic interactions" between biopolymers and low energy surfaces, J. Colloid Interface Sci., 111 (1985) 378–390.
[18] R.J. Good, C.J. van Oss, The modern theory of contact angles and the hydrogen bond components of surface energies, in: M.E. Schrader, G.I. Loeb, Modern Approaches to Wettability – Theory and Application, Springer Science+Business Media, New York, 1992.pp. 1–27.
[19] J.D. Berry, M.J. Neeson, R.R. Dagastine, D.Y.C. Chan, R.F. Tabor, Measurement of surface and interfacial tension using pendant drop tensiometry, J. Colloid Interface Sci., 454 (2015) 226–237.
[20] H.J. Busscher, H.C. van der Mei, Use of flow chamber devices and image analysis methods to study microbial adhesion, Methods Enzymol., 253 (1995) 455–476.
[21] S. Pohl, M. Madzgalla, W. Manz, H.J. Bart, *E.coli* biofilm characteristics on polymeric heat exchanger surfaces, Chem. Eng. Technol., 40(6) (2017) 1017–1024.
[22] R. Bos, H.C. van der Mei, H.J. Busscher, Physico-chemistry of initial microbial adhesive interactions – its mechanisms and methods for study, FEMS Microbiol. Rev., 23 (1999) 179–230.
[23] H.W. Fowler, A.J. McKay, The measurement of microbial adhesion, in: R.C. Berkeley et al., Microbial adhesion to surfaces, Ellis Horwood Ltd, Chichester, UK, 1980, pp. 141–163.
[24] A.J. García, P. Ducheyne, D. Boettinger, Quantification of cell adhesion using a spinning disk device and application to surface-reactive materials, Biomater., 18 (1997) 1091–1098.
[25] H. Schlichting, K. Gersten, Boundary Layer Theory, 8th ed., Springer, Berlin, Heidelberg, New York, 2000.
[26] M. Förster, Verminderung des Kristallisationsfoulings durch gezielte Beeinflussung der Grenzfläche zwischen Kristallen und Wärmeübertragungsfläche, University Braunschweig: PhD thesis, Cuvillier , Göttingen, 2001.
[27] E. Gaddis, Wärmeübergang und Rührleistung in Rührbehältern, in: VDI-Wärmeatlas, Springer, Berlin, Heidelberg, 2013, pp. 1621–1654.
[28] N.P. Boks, W. Norde, H.C. van der Mei, H.J. Busscher, Forces involved in bacterial adhesion to hydrophilic and hydrophobic surfaces, Microbiol., 154 (2008) 3122–3133.
[29] R. Baier, Adsorption of Microorganisms to Surfaces, Wiley-Interscience Publishers, New York, 1980.
[30] Q. Zhao, Y. Liu, C. Wang, S. Wang, H. Müller-Steinhagen, Effect of surface free energy on the adhesion of biofouling and crystalline fouling, Chem. Eng. Sci., 60 (2005) 4858–4865.
[31] S. Krishnan, C.J. Weinman, C.K. Ober, Advances in polymers for anti-biofouling surfaces, J. Mater. Chem., 18 (2008) 3405–3413.
[32] C. Dreiser, Falling Liquid Film Enhancement, Fouling Mitigation and Conceptual Design of Polymer Heat Exchangers, PhD thesis, University Kaiserslautern, 2016.
[33] R. Shang, A.R.D. Verliefde, J. Hu, S.G.J. Heijman, L.C. Rietveld, The impact of EfOM, NOM and cations on phosphate rejection by tight ceramic ultrafiltration, Sep. Purif. Technol., 132 (2014) 289–294.